applied optics

Wearable telescopic contact lens

Ashkan Arianpour,[1,*] Glenn M. Schuster,[1] Eric J. Tremblay,[4] Igor Stamenov,[1] Alex Groisman,[2] Jerry Legerton,[3] William Meyers,[3] Goretty Alonso Amigo,[3] and Joseph E. Ford[1]

[1]Department of Electrical and Computer Engineering, University of California San Diego, 9500 Gilman Drive, La Jolla, California 92093-0409, USA
[2]Department of Physics, University of California San Diego, 9500 Gilman Drive, La Jolla, California 92093-0409, USA
[3]Paragon Vision Sciences, 947 E. Impala Ave, Mesa, Arizona 85204, USA
[4]École polytechnique fédérale de Lausanne, Route Cantonale, 1015 Lausanne, Switzerland
*Corresponding author: aarianpo@ucsd.edu

Received 27 March 2015; revised 8 July 2015; accepted 11 July 2015; posted 13 July 2015 (Doc. ID 235760); published 11 August 2015

We describe the design, fabrication, and testing of a 1.6 mm thick scleral contact lens providing both 1× and 2.8× magnified vision paths, intended for use as a switchable eye-borne telescopic low-vision aid. The F/9.7 telescopic vision path uses an 8.2 mm diameter annular entrance pupil and 4 internal reflections in a polymethyl methacrylate precision optic. This gas-impermeable insert is contained inside a smooth outer casing of rigid gas-permeable polymer, which also provides achromatic correction for refraction at the curved lens face. The unmagnified F/4.1 vision path is through the central aperture of the lens, with additional transmission between the annular telescope rings to enable peripheral vision. We discuss potential solutions for providing oxygenation for an extended wear version of the lens. The prototype lenses were characterized using a scale-model human eye, and telescope functionality was confirmed in a small-scale clinical (nondispensed) demonstration.

OCIS codes: (110.6770) Telescopes; (170.4460) Ophthalmic optics and devices; (170.4470) Ophthalmology.

http://dx.doi.org/10.1364/AO.54.007195

1. INTRODUCTION

Age-related macular degeneration (AMD) is an aging-related ailment and the leading cause of blindness for individuals over the age of 55 [1], affecting an estimated 30–50 million patients worldwide. Some AMD patients rely on low-magnification telescopic visual aids, magnifying the object scene and increasing the effective image resolution in the region outside of the fovea [2]. These telescopes are typically field glasses attached to eyewear [3], requiring continuous head motion for viewing of extended scenes [4]. Recently, miniaturized telescopes have been surgically implanted into the crystalline lens of one eye, the other eye remaining unmodified [5]. These telescopes provide 2.2× or 2.7× magnification and a 20° field of view that moves with the direction of gaze. This eye-borne magnification allows for more natural eye movement and interpersonal interactions. However, the available volume inside the crystalline lens restricts the aperture to a relatively large F/# of 12.5, limiting effective use to well-lit environments.

A low-vision telescope in the form of a contact lens is a less invasive and more attractive solution. In 1963, an eye-borne 2× telescope was demonstrated as a visual aid for macular degeneration patients [6]. Two lenses and an aperture stop formed a refractive Galilean telescope, which was encapsulated within a 4.4 mm thick scleral contact lens. However, this lens is too thick to be worn comfortably, and simply scaling the refractive telescope to a sufficiently short length to fit comfortably would reduce the telescope aperture and resolution below a usable level.

A potential solution is to employ the geometry of a thin multiple-reflection telescope with an outer annular aperture [7]. This geometry has the advantage of reducing overall lens thickness by a factor equal to approximately the number of internal reflections, and also offers a central clear lens aperture which can be used to provide a separate optical path for unmagnified normal vision. We earlier described [8] a 1.1 mm thick switchable telescopic lens that provided both 1× and 2.8× magnification (Fig. 1) vision paths.

This lens was successfully fabricated and tested on a scale model of the human eye (Fig. 2). Adding an external linear polarizer to the 1× path, we demonstrated a basic level of switching by selectively blocking the 1× path with an orthogonal polarization and liquid crystal shutter. However, this first "Generation 0" lens was a proof-of-principle optic unsuitable for human use. The internal reflection telescope had sharp external edges which would need to be encapsulated within a smooth casing to be made wearable, which forces significant optical redesign. In addition, the cornea requires a continuous flow of environmental oxygen, as it lacks the blood vessels which oxygenate normal tissue. The 1.1 mm thick GEN 0 lens polymethyl methacrylate (PMMA) structure is impermeable to

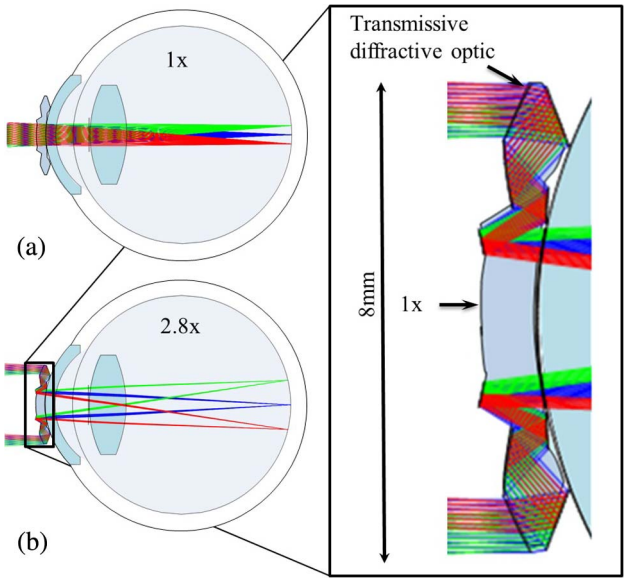

Fig. 1. Generation 0 (not wearable) reflective telescopic contact lens with (a) 1× and (b) 2.8× vision paths.

oxygen, allowing only short-term (less than one hour) wear before it would begin causing pain and potentially damage to the cornea.

This paper describes the design, fabrication, and testing of a version of this lens that is suitable for patients that suffer from a central scotoma of 5°–10° and is comfortable for human wear, at least for the short term. Methods are shown that can allow fabrication of a version compatible with extended wear. To do this, we require that the telescope be integrated as an optical "payload" embedded within the structure of a scleral lens and be modifiable to accommodate the user's vision correction prescription. We also changed the design to allow for switching between telescopic vision and a 1× vision mode that allows wide-field peripheral vision. The paper is organized as follows: Section 2 describes the proposed mechanical and optical design for the lens to be wearable on a human eye. Section 3 details the fabrication process and metrology regarding both the folded optic and scleral lens. Section 4 details the methods for testing the assembled scleral lens on an optomechanical eye model and the measured resolution for both unmagnified and telescopic vision. Section 5 describes the limitations of the fabricated optic, and Section 6 provides a demonstration of a proof-of-concept telescopic scleral lens in an exploratory clinical trial.

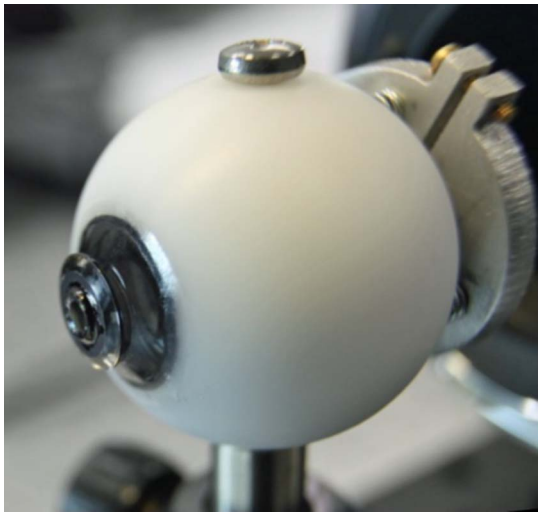

Fig. 2. Generation 0 (not wearable) telescopic contact lens on an optomechanical eye model used for testing.

2. WEARABLE LENS DESIGN

There are three major categories of contact lenses: the familiar soft contact lenses and the less common rigid lenses in both corneal and scleral lens form. Soft lenses are made of a flexible gas-permeable polymer, inexpensively mass produced by molding. The lenses are typically up to 14.5 mm in diameter and 84–230 μm thick [9]. Though comfortable to wear, these materials are too flexible to hold the telescope mirror surfaces with sufficient precision. Rigid corneal diameter lenses (typically 8–10 mm diameter) can support the telescopic surfaces but are too thin. Corneal lens thickness is constrained by user comfort because each time the user blinks, the eyelid must glide over the edge of the lens. They are also not accurately centered. Because the cornea surface is nearly spherical, corneal lenses allow significant lateral movement over the pupil. Scleral lenses are larger, typically from 12.9 to 24 mm in diameter [10], mounting on the white scleral region of the eye. Scleral lenses are commercially manufactured for special vision needs, including patients with highly irregular corneas. Each lens is diamond-turned to the user's physical eye geometry and vision prescription by companies such as Paragon Vision Sciences. Scleral lenses can be comfortable with center thicknesses up to 2 mm in thickness [11] because the user's eyelid remains on the scleral lens and does not need to glide over the edge of the lens when blinking. Second, because the sclera is not perfectly spherical, a properly designed scleral lens is more stable than a corneal lens in both lateral and rotational motion. [12].

Light collection of the concentric folded telescope is given by the area of the annular input aperture, which depends on the aspect ratio of the optic's thickness and the overall diameter, which is a function of the number of reflections used. A discussion of the scaling properties of concentric reflective imaging lenses can be found in [7], and the characteristics of an afocal telescope geometry are similar. Light collection increases with lens diameter which, given the constraints on aspect ratio, means that the lens center thickness also increases. Setting as a requirement a magnification close to 3×, we found that 2-reflection designs did not provide sufficient magnification and that 6-reflection designs and higher introduced too much aperture obscuration (and extremely tight tolerances). A 4-reflection lens with a center thickness of 1 mm (as in the GEN 0 lens) is necessary for sufficient resolution and light collection. The result is that a relatively thick scleral lens provides the most favorable geometry for the contact lens telescope optics.

A. Design for Oxygenation

Providing continuous oxygenation to the cornea is essential for both corneal and scleral contact lenses to be suitable for full-day wear. The GEN 0 lens was made of a standard PMMA optical

plastic, which is straightforward to diamond turn and mirror coat. PMMA is biocompatible, but it is also essentially impermeable to oxygen. One of the original goals of this research project was to investigate the use of rigid gas-permeable polymers for all of the internal lens structures. Optical designs using various gas-permeable polymer materials were successful, but the mirror coatings introduced two practical limitations. First, high-reflectivity mirror coatings themselves acted as oxygen barriers. The mirror can be made permeable using subwavelength patterning (i.e., a lossy subwavelength perforated pattern or nanostuctured plasmonic mirrors). But a second practical limitation was that the deposition of high-quality mirrors onto gas-permeable materials proved difficult. Mirrors of good quality were deposited but were not physically robust, and did not survive integration into the outer housing. More fundamentally, oxygen flow through 1 mm of even the most gas-permeable materials available was insufficient for reliable corneal oxygenation. Currently available rigid gas-permeable lenses provide sufficient oxygenation with Dk values ranging from 100 to 165 [13]. The most permeable rigid gas permeable (RGP) material available, Silicon Elastomer, has a Dk of 340, enabling thicknesses up to 0.71 mm [14]. But lens performance with this thickness constraint was unfavorable.

Given these challenges, we looked for solutions to oxygenation that would enable the central "payload" to be entirely gas impermeable. One possibility was to provide an oxygenated fluid under a substantially gas-impermeable lens. Perfluorocarbon liquids (PFCL) are one biocompatible candidate [15]. The 185 μl volume under a scleral lens may support a day-long reservoir of special PFCL contact lens solution. In addition, we investigated oxygenation via a structural as opposed to materials-based approach. Gas diffuses within a continuous open volume, even one with relatively small passages, significantly more easily than through even a thin layer of gas-permeable plastic, so we considered a contact lens that holds a gas-impermeable optical payload over a contiguous internal volume that extends over the cornea. Figure 3(a) shows the basic structure. Oxygen enters the watertight volume through a relatively thin outer cover that includes a significant surface area on the lens periphery. Oxygen consumed by corneal tissue is replaced by flow under the gas-impermeable payload through a similarly thin inner cover over the central (corneal) region. The overall structure is supported by internal supports between the inner and outer shells, as shown in Fig. 3(b). Since the surface area exposed to the outer air can be larger than the 10 mm diameter oxygen-consuming cornea, as long as diffusion under the gas-impermeable payload, the overall oxygen flow is substantially mediated by the thin layer over the cornea.

To verify this, we conducted simulations in COMSOL of a simplified worst-case model of an eye with a scleral lens and an impermeable "eyelid" partially covering part of the lens (Fig. 4). The model is of an aerated lens with the following features: (1) a circular surface at the center bottom, which is in contact with the cornea; (2) a thin layer of gas-permeable (RGP) material at the bottom (lower shell); (3) a thin cavity above the bottom RGP layer, providing the oxygenation to the cornea; (4) a layer of gas-impermeable material (folded optical elements of the lens) above this central area; (5) a gas-permeable top layer

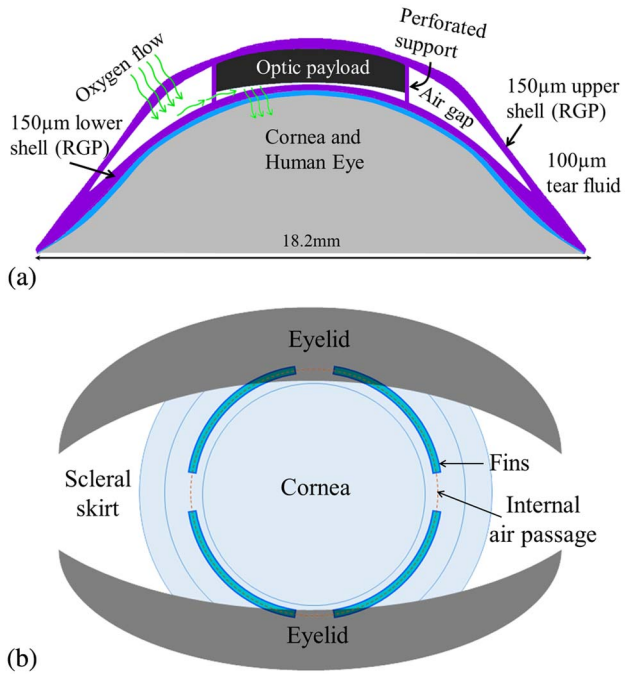

Fig. 3. (a) Schematic of air-gap solution for providing oxygenation to the cornea. (b) Geometry of eye with scleral lens, and distribution of fins (four in this case) along the structural support of the contact lens.

(upper shell); (6) a gas-impermeable outer cylindrical surface (that would not be present in the future real lens); (7) a gas-impermeable ring-shaped outer area at the bottom (the area in contact with the sclera, through which no net flow of O_2

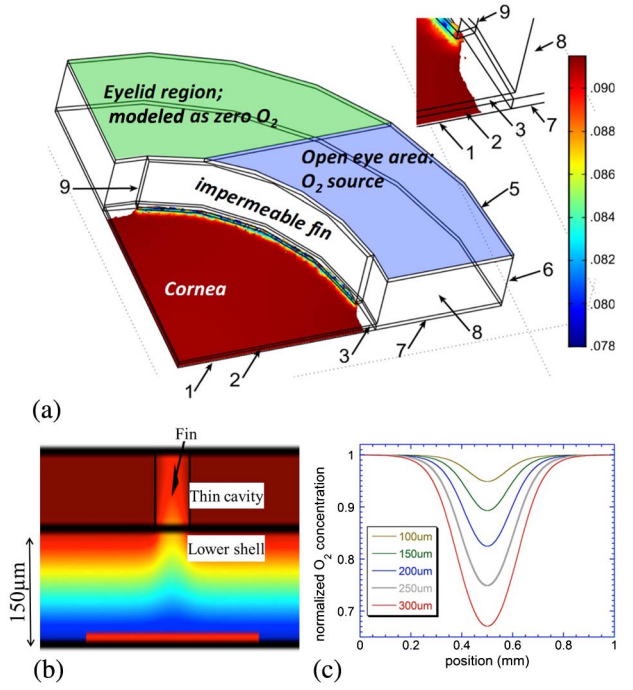

Fig. 4. (a) 3D COMSOL model of simplified air-gap geometry. (b) 2D model of air diffusion across perforated gap to the lower shell of the contact lens. (c) Normalized concentration of oxygen depending on cavity width.

occurs in the first approximation); (8) an annular void; and (9) an RGP partition between the central cylinder and the annular void, forming fins at the bottom. Another key parameter is the O_2 permeability of the RGP material of the lens. The RGP material is intended to be Paragon HDS 100, which has permeability of $\sim 100 \times 10^{-11}$ $cm^2/s \times [mL\ O_2/mL\ material \times mm\ Hg]$ which, for all purposes of our simulation (a steady-state situation), is equivalent to a combination of 100% solubility and a diffusion coefficient of 0.76×10^{-6} cm^2/s. The O_2 transport is from the atmosphere through the outer ring-shaped region of the upper shell (above the annular void), through the annular void region (8), towards the thin air cavity (3), and from the air cavity through the lower shell (2) towards the cornea (1). The simulation results indicate a nearly uniform distribution of the O_2 concentration over a plane at 30 μm distance from the bottom surface of the lens in the 11 mm diameter circle just above the cornea, other than in the immediate vicinity of the fin. The ∼0.090 value of the O_2 concentration at the 30 μm distance suggests that the transport of O_2 towards the bottom of the lens (cornea) is equivalent to the O_2 transport though a uniform layer of the solid RGP material with a thickness of 30 μm/0.090 = 333 μm. Such a layer of HDS 100 can be potentially reduced to be consistent with common contact lens practice to ensure sufficient oxygenation of the cornea.

Azimuthal variations of the O_2 concentration are minimal as well, suggesting that it is sufficient to have just four openings connecting the annular void with the thin cavity above the cornea. Using a larger number of openings would further improve the azimuthal uniformity. We also performed 2D numerical simulations for the same RGP material to account for changes in the O_2 transport due to fins that may be introduced into the thin cavity to make it more structurally stable [Fig. 4(b)]. An actual fin will have a finite length. Therefore, the 2D simulation is the worst-case scenario for the reduction in the O_2 transport. A proxy for the O_2 transport rate is the O_2 concentration at a given short distance above the bottom of the lower shell (10 μm). The simulation indicates maximal reductions of the local transport rate by 5%, 11%, 17.5%, 25%, and 37% for 100, 150, 200, 250, and 300 μm wide fins, respectively. So for example, adding a 250 μm wide fin in an internal area of the thin cavity in the lens will reduce the local O_2 transport under the center line of the fin to a rate equivalent to that through a uniform 400 μm thick slab of RGP.

These calculations indicate the potential effectiveness of this structure to provide oxygen, and the introduction of a thin internal air gap on the optical functionality has a negligible impact on optical performance, as will be demonstrated in the following section. This fabrication of this structure is, however, a significant technical challenge. A research effort on this topic is underway and will be reported separately. For the remainder of this paper, we will concentrate on the design and prototyping of the lens structure compatible with the air gap oxygenation for extended wear, and with a solid lens structure for short-term clinical evaluation of performance.

B. Optical Design

The key difference between the contact lens telescopes and the previous work on 4- and 8-reflection imaging lenses is that the imagers used a substantially planar front surface, while the contact lens input aperture must follow the curvature of the eye's surface. This is important for the optical design because the initial refraction at the lens input introduces color-dependent optical power whereas the subsequent internal reflections are intrinsically wavelength independent. No combination of simple mirrors can correct for the significant initial chromatic aberration introduced by the curved input face. The Gen 0 telescope (Figs. 1 and 2) used a surface relief diffractive kinoform structure to correct this axial color, but such a structure cannot be used with a wearable lens. Tears from the eye would form a tear film over the lens, smoothing the diffractive surface to reduce both diffraction efficiency and the chromatic correction, and the surface relief structure would also cause discomfort for the wearer when blinking. The diffractive kinoform in the PMMA substrate can be hidden below a covering layer of index n_{cover}, but this would require increasing the depth of the features from $\lambda/(n_{PMMA} - 1) = \sim 1$ μm to $\lambda/(n_{PMMA} - n_{cover}) = \sim 10$ μm, increasing the usable lateral feature size above the length required for color correction. It could also be fabricated on the first reflective surface, which would require the depth of the multilevel or analog features be reduced to $\lambda/2n_{PMMA} = \sim 0.1$ μm, which would require excessive precision in the step size.

Instead, the wearable lens we investigated uses refractive color correction by a combination of PMMA "crown" ($n = 1.49$, Abbe number 58) and Paragon's HI-154 rigid gas-permeable contact lens material, which has a high refractive index and relatively high dispersion ($n = 1.54$, Abbe number 29), acting as our "flint." The optical design of the new lens is shown in Fig. 5. This lens is designed using the immersed fused silica elements and curved focal surface of our model eye (as in Fig. 1), which will be described in Section 4.A, including Fig. 11, and [16]. The normal 1× vision path through the 2.6 mm diameter (21.2 mm^2 area) central circular aperture provides F/# 4.1 vision. The 2.8× magnified vision path through the annular input with 4.1 mm outer and 2.78 mm inner radius (28.5 mm^2 in area), provides F/# 9.7 vision. The four reflections introduce additional loss on the telescopic path, so the T/# for this path can be higher depending on fabricated mirror reflectivity. The central path uses substantially spherical surfaces with a small, even aspheric correction. The annular telescopic path relies on high-order aspheres to correct for optical aberrations in a limited optical path length. The prescription of the scleral lens can be modified for any user by adjusting the power of the input surfaces for the 1× and 2.8× paths, including spherical power to correct for myopia or hyperopia, and cylindrical power to correct for astigmatism.

In the fabrication process used to make the first "GEN 1" lens, areas between and around the annular rear mirrors were also mirror coated, creating some reflective nonoptical surfaces. Reflections from these surfaces do not enter the eye, but these surfaces do block off-axis light [Fig. 6(a)]. All light from the object scene needed to pass through the 1× aperture, and axial offset of the 2.6 mm entrance aperture from the internal pupil of the eye caused considerable vignetting of the 1× vision path. The fabrication process used in a second fabrication of a "GEN 2" optic (as described in the following section) was revised to

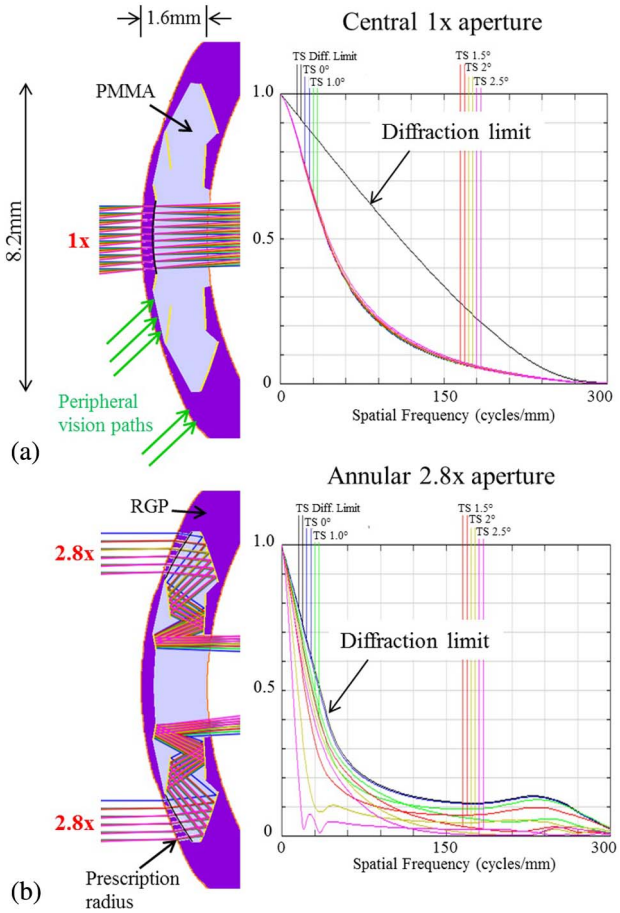

Fig. 5. Schematics of the scleral contact lens with polychromatic modulation transfer function (MTF) calculations on a model eye with a pupil of 4 mm for (a) 1× unmagnified vision and (b) 2.8× telescopic vision.

increase the field of view of the 1× path. This removed the unnecessary mirrors and filled the regions with a material of the same refractive index as the PMMA substrate for the folded optic, providing unaberrated pathways for peripheral vision as shown in Fig. 6(b).

Reflective optical surfaces have intrinsically tighter tolerances than refractive surfaces, so control of the surface and alignment tolerances is crucial in the four-reflection single-part structure and aspheric reflectors. The inner "insert" is particularly sensitive to front-to-back thickness, centration, and wedge errors since the part has to be re-chucked during diamond turning. These tolerances were included in the design process by optimizing simultaneously over four different configurations (1) an unaltered version, (2) a version with 5 μm decenter error front to back, (3) a version with a 5 μm thickness error, and (4) a version with a 0.010° surface tilt front to back. This joint optimization helped us to find design solutions with acceptable sensitivity to the expected fabrication errors.

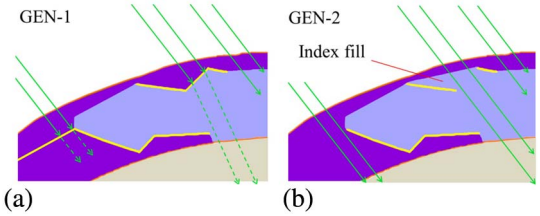

Fig. 6. Close-up of (a) GEN 1 scleral lens and (b) GEN 2 scleral lens, which allows peripheral vision via light between the mirrors.

For compensation for the thickness tolerance, we allowed an adjustment of the front curvature of the outer scleral lens before its final shaping based on the measured thickness of fabricated insert parts. This method helps avoid a stack up of the thickness tolerances, which are otherwise difficult to control. We found that a part thickness error of up to 10 μm could be corrected with <1.2 diopters of front correction. We chose to limit the allowable thickness error to 5 μm to better maintain compensated performance.

The tolerances shown in Tables 1 and 2 maintain diffraction-limited performance on-axis and <5% drop in MTF across the field.

3. FABRICATION AND ASSEMBLY PROCESS

In this section, we concentrate on the fabrication and test of a lens for short-term wear. Figure 7 shows the components and assembly steps for the GEN 2 switchable telescopic scleral lens. The center of the lens is a PMMA diamond-turned insert ("precision telescope insert") with enhanced aluminum-coated annular mirrors. This element was fabricated by ISP Optics using a 250 UPL single-point diamond lathe. This part needs to be surrounded by complementary-shaped PMMA and HI-154 index fills. The telescope insert is placed between a top PMMA index fill and a bottom HI-154 index fill diamond turned by Paragon Vision Sciences using an Optoform 40 ophthalmic lathe, forming a solid cylindrical "triple stack." The parts were bonded by Dymax 141-M, a flexible medical UV-cure adhesive with refractive index 1.49, similar to the index of PMMA. This stack is then diamond-turned to a "shaped post," where the only part of the top index fill that remains is a thin layer between the top two annular mirrors. This volume is necessary to avoid distortion of the peripheral vision path.

In a future assembly process, two orthogonal polarizers that cover the unmagnified and telescopic vision paths will be bonded to the shaped-post surface to enable a polarization-based switching mechanism. A top handle composed of HI-154 is then bonded to the shaped post using Dymax 210CTH, a more rigid medical UV-cure adhesive, imbedding

Table 1. Precision Insert Fabrication Tolerances

Front-to-back decenter (μm)	±5
Front-to-back thickness (μm)	±5
Front-to-back wedge (μm)	±5
Individual reflector thickness (μm)	±3
Individual reflector tilt (deg)	±0.01

Table 2. Outer Scleral Lens Tolerances

Thickness (μm)	±25
Surface tilt (deg)	±0.075
Radius of curvature	±0.100

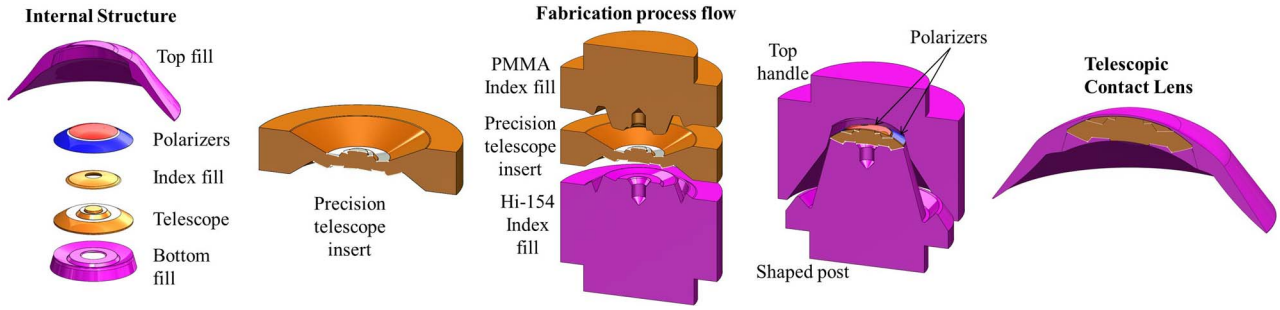

Fig. 7. Left to right: Components for scleral contact lens, diamond-turned PMMA and aluminum-coated precision telescope, triple stack to form index fill for peripheral region, post cut for polarizer attachment and HI-154 shells, and final telescopic contact lens.

the index filled telescope between two high-refractive-index parts that provide achromatic correction and the overall scleral lens shape. Finally, this part is diamond-turned into the scleral lens based on the wearer's physical and optical prescription. Figures 8(a) and 8(b) show the triple-stack components prior to bonding, and the post cut, including the PMMA index fill. Figures 8(c) and 8(d) show the completed scleral lens where the annular rings appear to be "floating" in the PMMA medium, where the transparent spaces between the mirrors provide the peripheral vision path. The completed optic is 18.2 mm in diameter, with a center thickness of 1.6 mm. Figure 9 shows a cross-section of one of the completed lenses, revealing the glue line thicknesses and the quality of the match between the insert and the HI-154 material. The adhesive seam is uniform over the input aperture, with a 35 μm thickness determined by the uncured adhesive's viscosity and the physical match between the shaped parts, which are designed to come in contact at the shoulders outside the input aperture. We measured the dimensions of the inserts, complementary parts, and assembled prototype using profilometers and a laser scanner, examining the cross-sections of all components and final assembly. All specs were measured to be accurate within the tolerances of the metrology itself, except for surface roughness of the input surface and the mirrors (Fig. 10).

4. IMAGING PERFORMANCE

A. Quantifying Resolution

The resolution of the telescopic scleral lens was measured using an optomechanical fluid-filled eye model with a full field of view of 34° (Fig. 11) [16]. The design of the eye model optics was derived from the Navarro eye model, with fused silica single elements with conic surfaces for both the cornea and crystalline lenses. Distilled water fills the regions between the 1.458 index lenses to replicate the aqueous and vitreous humors of the human eye. The imaging surface is a fiber bundle with 4.2 μm pitch, and does not limit the resolution of the measurement. The fibers transmit the focused object scene from the curved input face to the planar output, where the image is emitted into free space and then photographed using relay optics and a Canon DSLR camera.

The scleral lens is placed on the cornea of the eye model with distilled water and is held in place by surface tension. Figure 11(b) shows circular and annular apertures positioned in front of the scleral lens and alternated to enable switching between normal and telescopic vision. Measurements were conducted to ensure the optic was not decentered, and that the 1× and 3× vision paths were aligned with the on-axis region of the eye model and fiber bundle. The object scene was placed

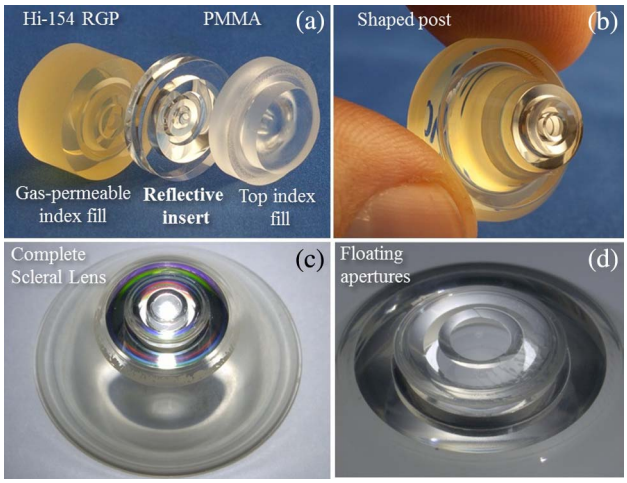

Fig. 8. (a) Unassembled triple stack of scleral lens components. (b) Cut post with PMMA index fills. (c) Complete scleral lens. (d) Close-up of floating apertures for peripheral regions.

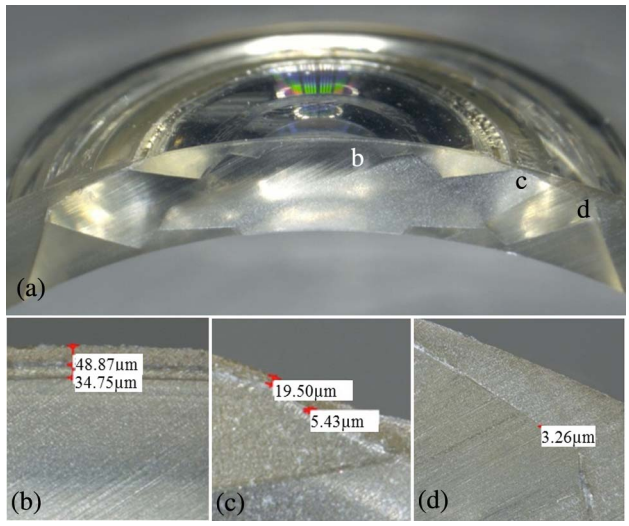

Fig. 9. Cross-section and thicknesses of HI-154 shells and glue lines of the scleral lens.

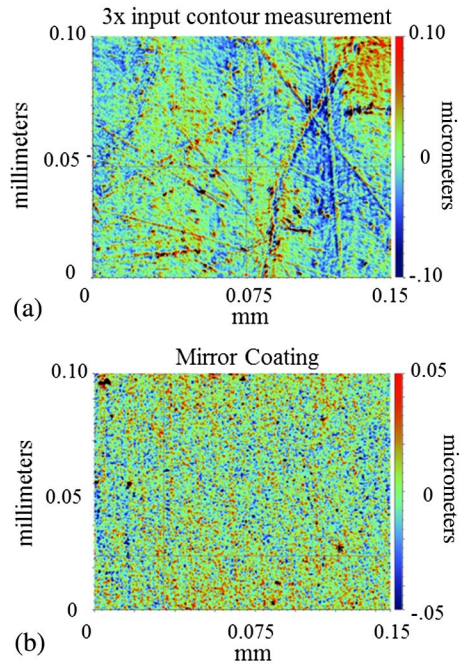

Fig. 10. Veeco white light interferometer scan of (a) the scleral lens 2.8× input surface and (b) the relatively smooth mirror-coated telescope inserts (note the 2× smaller depth color scale).

approximately 6 meters away from the testing apparatus, and images were captured for both the 1× and 2.8× path. The eye model is focused by moving the curved-face fiber bundle along the optical axis to the optimum position for the telescopic path.

Figure 12 shows images acquired of the 1× and 2.8× telescopic path, where the eye was focused to obtain the best 2.8× image. The on-axis MTF of the optical system (Fig. 13) was measured using a slant-edge pattern and Imatest software. Resolution for the telescopic path was significantly lower than

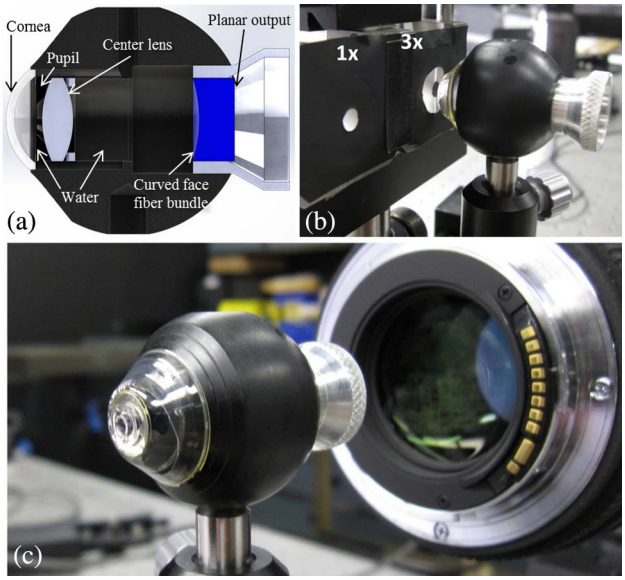

Fig. 11. (a) Modeled cross-section of testing apparatus for HFZ lens. (b) Switching between 1× and 2.8× vision. (c) Relay imaged to camera.

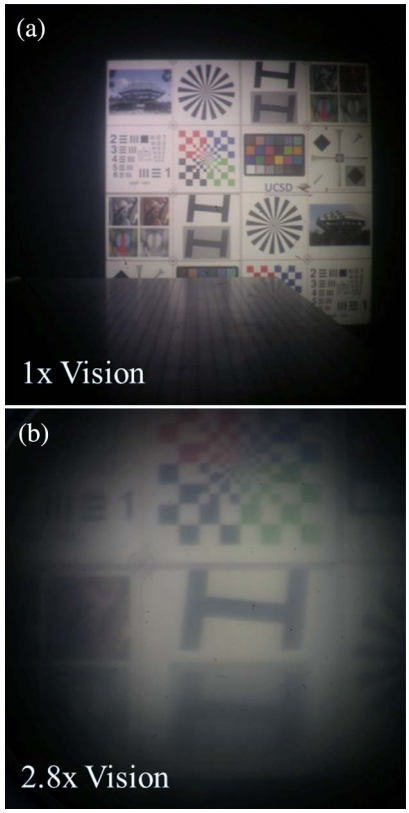

Fig. 12. Image results of HFZ lens on eye model. (a) 1× path taken at 0.6 s exposure and 100 ISO and (b) 2.8× path taken at 2.0 s exposure and 100 ISO.

the theoretical design (Fig. 5), with an average horizontal and vertical MTF10 of 13 cycles/mm. The drop in 2.8× path resolution will be discussed further in Section 5. The resolution of unmagnified vision path has also dropped by comparison to the bare eye model [16], as the best focus for the telescopic vision path was approximately 100 μm away from the 1× vision best focus. Focusing for the unmagnified vision path achieves an MTF10 of 103 cycles/mm, or 20/20 equivalent vision, according to design [17].

B. Peripheral Vision Testing

The 34° field of view of the eye model covers a region larger than the fovea, but is inadequate for testing the peripheral vision. A simplified optical system that approximates the focal length and F/# of the eye was used to quantify the transmission of light through the peripheral vision paths as a function of angle (Fig. 14). The GEN 1 and GEN 2 lenses were positioned in front of a biconvex lens with a focal length (18 mm) (nearly equivalent to the human eye) and an aperture of 4 mm (similar to the nominal pupil size). The distance between the scleral lenses and the biconvex lens was approximately 4.5 mm to replicate the anterior chamber depth of the eye. A 5 megapixel CMOS imager was placed at the focal point of the system and measured the intensity of the transmitted light which could pass through the 1× aperture, through the peripheral index-matched regions (between the annular reflectors), and through the edge of the scleral lens' skirt [Fig 14(b)]. The normalized

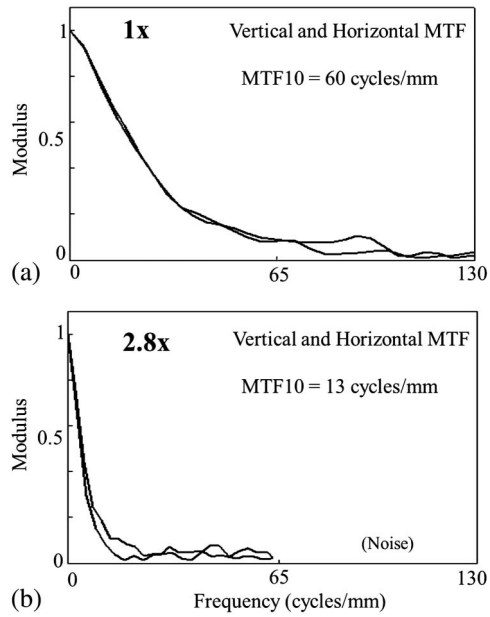

Fig. 13. Slant edge MTF measurements for both (a) 1× path and (b) 2.8× path, with the lens set at best focus for the 2.8× path.

transmission intensity as a function of angle was measured by varying both the angle of illumination of the white light source and the position of the sensor. Figure 14 shows that the GEN 1

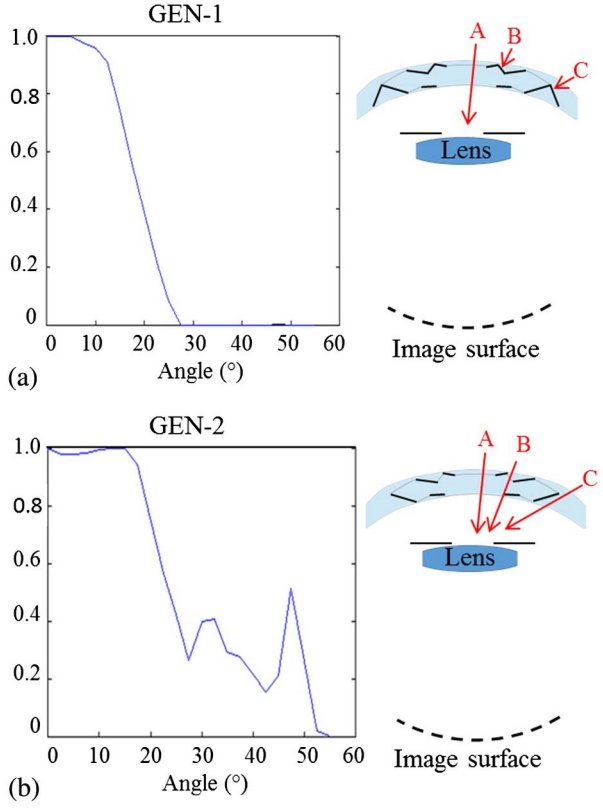

Fig. 14. Measurement of the transmission of the peripheral path in (a) GEN 1 contact lens, and (b) GEN 2 contact lens. The red lines labeled "A, B, C" illustrate the transmission paths for peripheral vision.

contact lens' nonoptical mirrored regions prevented the transmission of light at large angles, limiting peripheral vision to well below 30°. However, the floating annular mirrors and PMMA index-filled regions of the GEN 2 lens allow for light transmission at larger angles, providing peripheral vision up to 55° and nearly doubling the field of view of the GEN 1 design.

5. LIMITATIONS TO RESOLUTION

The measured resolution of the 2.8× path, while well below the design illustrated in Fig. 5, is at a level which may be useful as a low-vision aid for AMD patients. However, the resolution may be primarily constrained by the final fabrication step, the shaping of the outer lens surface to the wearer prescription. This step was done by Optoform 40 diamond turning, using processes that are standard for scleral contact lens manufacturing. However, the 2.8 magnification of the folded optic is more sensitive to fabrication errors, including surface roughness. Measuring a larger region of the air–polymer telescopic path's input surface revealed an (Ra) = 23 nm with peak-to-valleys of 150 nm (Fig. 15). The roughness of the surface profile for the telescopic path was approximated by integrating along the arrowed line on the measured surface plot, followed by tiling the measurement a total of 4 times in series from one another. This approximated roughness profile was used to modulate the designed input surface and calculate the MTF of the roughened surface, and is shown by the red line in Fig. 16. Additionally, Fig. 16 shows a plot for a roughness that is reduced by a factor of 1/5th, and observed an improvement in the system's MTF. Therefore, we believe that the drop in resolution is caused by surface roughness of both the input surface of the scleral lens and the mirror coating on the diamond-turned insert. The performance of the system can possibly be improved by switching to higher-precision diamond-turning technology. Standard

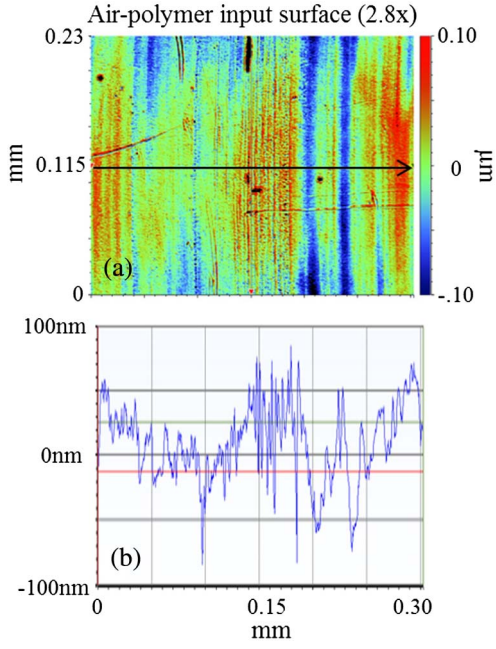

Fig. 15. (a) Veeco white light interferometer regional 2D measurement of 2.8× path. (b) line profile across 2D scan.

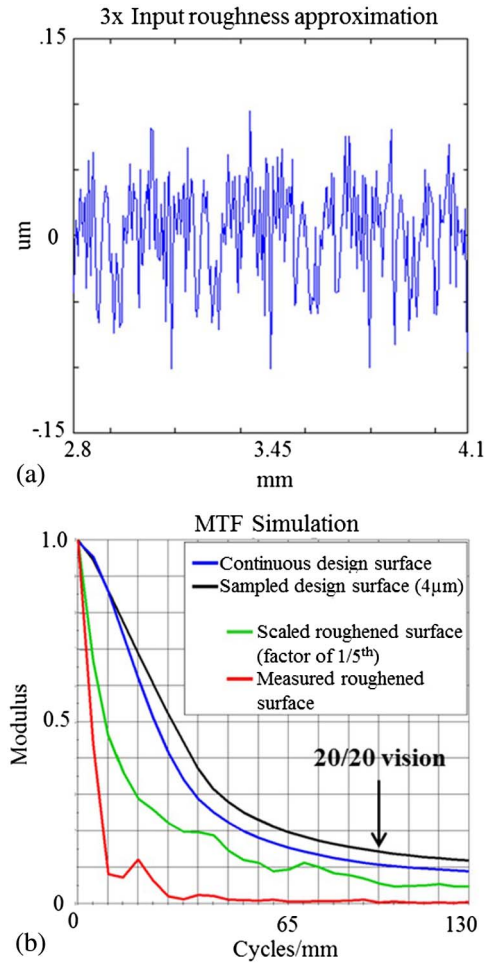

Fig. 16. (a) Approximation of surface roughness across 3× profile from Veeco interferometer scan. (b) FRED MTF calculation for roughened 2.8× path surface profile.

commercial contact lens equipment can rapidly fabricate contact lenses for custom prescriptions with accuracies sufficient for conventional vision correction. However, a higher-performance telescopic lens may require advanced diamond turning (or post polishing) for the final lens shaping.

Stray light was also examined by considering multiple paths through the reflective optic, including those that bypass one or more of the mirrors, and was found to lie outside of the field of view of the 3× image.

6. CLINICAL FEASIBILITY TEST

A small-cohort clinical study, approved by the Naval Medical Center San Diego Institutional Review Board and the Department of Defense Human Research Protections Office, was conducted on a single eye of five adult subjects. The subjects were volunteers with normal vision other than myopia or hyperopia. The clinical supplies were the telescopic-only GEN 1 scleral lenses. The lenses did not have the mechanism for providing oxygen to the cornea and, as a result, the subjects wore the contact lens for a short period of time (~30 min). The investigational lenses were measured and found to not have optics that were reduced in quality due to mirror adhesion and surface roughness. A decision was made to proceed in an effort to measure the centration, movement, comfort, and presence or absence of magnification.

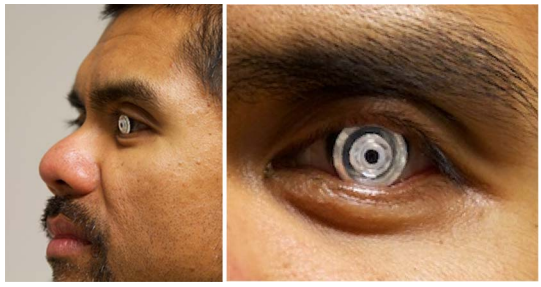

Fig. 17. Clinical test subject wearing the GEN 1 contact lens.

The lenses were applied (Fig. 17), and allowed to equilibrate for 15 min. The lenses demonstrated centration horizontally and an average of 0.5 mm displacement below the geometric center of the pupil. The lenses were stable and were observed to have less than 0.2 mm movement on the blink. All subjects reported the lens comfort to be good or very good. As expected, the subjects reported their vision to be blurred, but reported magnification when comparing the image size with the contact lens to that of their eye without the contact lens.

The results from this small exposure sample with the non-optimized optics and absence of the oxygen mechanism support the feasibility of the scleral lens platform to deliver a well-centered, stable, and comfortable form factor for telescopic magnification.

7. CONCLUSION

In conclusion, we have demonstrated the optical design and fabrication of a wearable eye-borne telescope in the form of a scleral contact lens. The lens was tested in the laboratory using a life-sized model eye, and shown to image both 1× and 2.8× vision paths. We show modeling results that indicate that the 2.8× path resolution was limited by fabrication tolerances, most notably the surface finish on the input aperture. This surface finish may be improved using higher-precision diamond turning or post-polishing of the lens surface. An initial form of the lens was tested in a small-scale clinical demonstration on human subjects. This initial lens was oxygen impermeable, and oxygen delivery to the cornea is a subject of further research and development. We described two methods that can lead to an extended-wear version of the lens. Another subject of ongoing work is the integration of spatially patterned polarizers to distinguish between 1× and 2.8× vision paths, as well as self-contained polarization-switching eyewear that will allow hands-free switching between magnifications.

Funding. Defense Advanced Research Projects Agency (DARPA) (W911NF-11-C-0210).

REFERENCES

1. D. S. Friedman, B. J. O'Colmain, and I. Mestril, "2012 Fifth Edition of Vision Problems in the U.S.," http://www.visionproblemsus.org/introduction/acknowledgments.html.

2. C. Dickinson, *Low Vision: Principles and Practice* (Butterworth-Heinemann, 1998).
3. http://www.eschenbach.com/consumers-low-vision-devices-for-the-visually-impaired.htm.
4. J. P. Szlyk, W. Seiple, D. J. Laderman, R. Kelsch, J. Stelmack, and T. McMahon, "Measuring the effectiveness of bioptic telescopes for persons with central vision loss," J. Rehabil. Res. Dev. **37**, 101–108 (2000).
5. S. S. Lane and B. D. Kuppermann, "The implantable miniature telescope for macular degeneration," Curr. Opin. Ophthalmol. **17**, 94–98 (2006).
6. A. Isen, "Feinbloom miniscope contact lens," in *Encyclopedia of Contact Lens Practice* (International Optics, 1963), Vol. **3**, Suppl. 13, pp. 53–55.
7. E. Tremblay, R. Stack, R. Morrison, and J. Ford, "Ultrathin cameras using annular folded optics," Appl. Opt. **46**, 463–471 (2007).
8. E. J. Tremblay, I. Stamenov, R. Beer, A. Arianpour, and J. Ford, "Switchable telescopic contact lens," Opt. Express **21**, 15980–15986 (2013).
9. http://www.acuvue.com/sites/default/files/content/us/pdf/M-09-14-00%201DAVM%20PI-FIG%20(website).pdf.
10. http://www.acculens.com/Acculens%20Webinar%20March.pdf.
11. http://www.sclerallens.org/about.
12. http://www.reviewofoptometry.com/continuing_education/tabviewtest/lessonid/108308/.
13. W. Benjamin and Q. Cappelli, "Oxygen permeability (Dk) of thirty-seven rigid contact lens materials," Optom. Vis. Sci. **79**, 103–111 (2002).
14. http://www.bausch.com/ecp/our-products/contact-lenses/aphakia/silsoft-and-silsoft-super-plus#.VPJoi_nF_0c.
15. Y. Imamura, M. Minami, M. Ueki, B. Satoh, and T. Ikeda, "Use of perfluorocarbon liquid during vitrectomy for severe proliferative diabetic retinopathy," Br. J. Ophthalmol. **87**, 563–566 (2003).
16. A. Arianpour, E. J. Tremblay, I. Stamenov, J. E. Ford, D. J. Schanzlin, and Y. Lo, "An optomechanical model eye for ophthalmological refractive studies," J. Refract. Surg. **29**, 126–132 (2013).
17. H. Gross, F. Blechninger, and B. Achtner, *Handbook of Optical Systems, Survey of Optical Instruments* (Wiley, 2008).